Mon. Not. R. Astron. Soc. **371,** 1125–1139 (2006) doi:10.1111/j.1365-2966.2006.10785.x

Feedback and metal enrichment in cosmological SPH simulations – II. A multiphase model with supernova energy feedback

C. Scannapieco,[1,2⋆] P. B. Tissera,[1,2⋆] S. D. M. White[3⋆] and V. Springel[3⋆]

[1]*Instituto de Astronomía y Física del Espacio, Casilla de Correos 67, Suc. 28, 1428, Buenos Aires, Argentina*
[2]*Consejo Nacional de Investigaciones Científicas y Técnicas, CONICET, Argentina*
[3]*Max-Planck Institute for Astrophysics, Karl-Schwarzchild Str. 1, D85748, Garching, Germany*

Accepted 2006 July 7. Received 2006 July 3; in original form 2006 April 6

ABSTRACT

We have developed a new scheme to treat a multiphase interstellar medium in smoothed particle hydrodynamics simulations of galaxy formation. This scheme can represent a co-spatial mixture of cold and hot ISM components, and is formulated without scale-dependent parameters. It is thus particularly suited to studies of cosmological structure formation where galaxies with a wide range of masses form simultaneously. We also present new algorithms for energy and heavy element injection by supernovae, and show that together these schemes can reproduce several important observed effects in galaxy evolution. Both in collapsing systems and in quiescent galaxies our codes can reproduce the Kennicutt relation between the surface densities of gas and of star formation. Strongly metal-enhanced winds are generated in both cases with ratios of mass-loss to star formation which are similar to those observed. This leads to a self-regulated cycle for star formation activity. The overall impact of feedback depends on galaxy mass. Star formation is suppressed at most by a factor of a few in massive galaxies, but in low-mass systems the effects can be much larger, giving star formation an episodic, bursty character. The larger the energy fraction assumed available in feedback, the more massive the outflows and the lower the final stellar masses. Winds from forming discs are collimated perpendicular to the disc plane, reach velocities up to $\sim$1000 km s^{-1}, and efficiently transport metals out of the galaxies. The asymptotically unbound baryon fraction drops from >95 per cent to $\sim$30 per cent from the least to the most massive of our idealized galaxies, but the fraction of all metals ejected with this component exceeds 60 per cent regardless of mass. Such winds could plausibly enrich the intergalactic medium to observed levels.

Key words: methods: *N*-body simulations – galaxies: abundances – galaxies: evolution – galaxies: formation – cosmology: theory.

1 INTRODUCTION

Within the current cosmological paradigm, galaxies form in a hierarchical fashion. Small systems collapse first, and larger systems build up through accretion both of diffuse material and of pre-existing objects. The variety of physical processes involved in this assembly, their complex non-linear interplay, and the broad range of scales over which they act, make detailed study of galaxy formation a challenging task. Numerical simulations which can treat both collisionless and dissipational dynamics provide a powerful tool to address this problem. With simple recipes for star and black hole formation and for feedback from supernovae (SNe), stellar winds and active galactic nuclei (AGN), they allow physically based studies of galaxy formation from the initial conditions posited by the concordance Lambda cold dark matter (ΛCDM) cosmology. However, significant numerical challenges arise in this approach because of the need to describe simultaneously the large-scale dynamics of protogalactic assembly and the small-scale processes associated with the formation and evolution of stars.

A major limitation of the popular smoothed particle hydrodynamics technique (SPH; Gingold & Monaghan 1977; Lucy 1977) is its inability to represent multiphase, multiscale mixtures like the interstellar medium (ISM) in star-forming galaxies. In the SPH formalism, the density associated with a given particle is estimated by averaging over all neighbours within an adaptively defined smoothing region. In a multiphase ISM most of the volume is filled with hot, diffuse gas while most of the mass lies in cold, dense clouds with sizes and masses which cannot be resolved in a galaxy-scale

⋆E-mails: cecilia@iafe.uba.ar (CS); patricia@iafe.uba.ar (PBT); swhite@mpa-garching.mpg.de (SDMW); volker@mpa-garching.mpg.de (VS)

simulation. The density associated with 'hot' particles is then overestimated because some 'cold' particles lie within the smoothing kernel. This results in overestimation of the associated cooling rate, excessive condensation of cold gas, and too high a star formation rate (Thacker et al. 2000; Pearce et al. 2001). Several ad hoc 'solutions' of differing complexity have been suggested for this problem. Hultman & Pharasyn (1999) used a two-phase ISM which comprises a hot-gas component and cold clouds. These two phases interact with each other through radiative cooling and evaporation of the cold clouds. Pearce et al. (1999, 2001) explicitly decoupled cold and hot phases defined by pre-set characteristic temperature boundaries. Thacker & Couchman (2001) reduced overcooling by allowing no radiative losses for 30 Myr from particles which had just been heated by SNe, thereby allowing a wind to develop. Springel & Hernquist (2003) developed an analytic subresolution model for the regulation of star formation in a multiphase ISM, and inserted galactic winds of given velocity and mass-loss rate 'by hand'. More recently, Harfst, Theis & Hensler (2006) also used a two-phase ISM and assumed a variable star formation efficiency depending on the ISM properties. In this paper, we present a new multiphase SPH scheme, similar to that of Marri & White (2003), in which particles with very different thermodynamic variables do not see each other as neighbours. Our model decouples phases with very different specific entropies, based on a local comparison of particle pairs. This allows hot, diffuse gas to coexist with cold, dense gas without introducing ad hoc characteristic scales.

The relevance of SN feedback for the evolution of galaxies has been emphasized by numerous observational and theoretical studies. SNe are the main source of heavy elements in the Universe and the presence of such elements substantially enhances the cooling of protogalactic gas (e.g. White & Frenk 1991). On the other hand, the release of energy by SNe heats up the surrounding material, leading to disruption of cold gas clouds and to reduced star formation. This energy can drive enriched material into the outer regions of galaxies or even transport it into the intergalactic medium (IGM; Lehnert & Heckman 1996; Dahlem, Weaver & Heckman 1998; Rupke, Veilleux & Sanders 2002; Frye, Broadhurst & Benítez 2002; Martin 2004; Shapley et al. 2004). Small systems are thought to be more strongly affected by SNe because of their shallower potential wells which are less efficient in retaining baryons (Larson 1974; White & Rees 1978; Dekel & Silk 1986; White & Frenk 1991). The joint action of chemical enrichment and hydrodynamic heating by SNe is often referred to as 'feedback'. Feedback structures the ISM, establishes a self-regulated cycle for star formation, and ultimately explains the detailed luminosities of galaxies as well as the origin of heavy elements in the IGM and elsewhere. Recent work has emphasized that feedback from AGN may also play a critical role in shaping galaxy evolution (e.g. Di Matteo, Springel & Hernquist 2005; Croton et al. 2006). For simplicity, we do not consider such processes in the current paper.

The treatment of SN feedback in simulations of galaxy formation is complicated by the fact that the physical mechanisms which inject energy and heavy elements into the ISM act on unresolved scales. Consequently, recipes must be implemented that correctly mimic their combined effects on scales that are resolved. In recent years, a number of authors have developed star formation and feedback recipes for simulating galaxy formation with both mesh-based and SPH codes (e.g. Katz & Gunn 1991; Cen & Ostriker 1992; Navarro & White 1993; Metzler & Evrard 1994; Yepes et al. 1997; Cen & Ostriker 1999; Sommer-Larsen, Gelato & Vedel 1999; Kay et al. 2002; Lia, Portinari & Carraro 2002; Semelin & Combes 2002; Marri & White 2003; Springel & Hernquist 2003). These studies have shown that simply injecting the energy into the thermal reservoir of surrounding gas is ineffective, producing negligible effects on the hydrodynamics. This is because stars form (and explode) in high-density regions where gas cooling times are short. The injected energy is thus radiated before it can drive significant motions (Katz 1992). Such thermal feedback is unable to regulate the star formation activity or to drive the kind of winds observed in starbursting galaxies.

Several alternative schemes have been proposed to produce more effective feedback in simulations. For example, Navarro & White (1993) suggested investing the SN energy directly in outward motions imposed on surrounding gas. Gerritsen & Icke (1997) turned off cooling for a brief period after particles acquire feedback energy, allowing them to evolve only adiabatically over this time (see also Mori et al. 1997). Thacker & Couchman (2000) implemented a similar recipe, adjusting the density of heated particles in order to prevent immediate energy losses. More recently, Springel & Hernquist (2003) added galactic winds to their multiphase model by explicitly creating wind particles at a rate proportional to the star formation rate and assigning them a predefined outward 'wind' velocity. While each of these approaches has had some success, it is clear that all have arbitrary ad hoc elements and none is fully satisfactory. In particular, all of them introduce characteristic values for wind speeds, mass injection rates, flow times or other parameters which should, in principle, be set by the dynamics of the system and which are likely to vary substantially between systems of different scale, metallicity, etc. Given the central importance of feedback, it remains an important task to improve the numerical treatment of this process in our simulations.

In this paper, we implement energy and chemical feedback in the context of our multiphase model for the ISM. Our new energy feedback scheme supplements the treatment of chemical enrichment already discussed in Scannapieco et al. (2005, Paper I), and is also implemented in the parallel TreeSPH code GADGET-2 (Springel 2005). Our primary goal is to address some of the shortcomings of previous implementations within a comprehensive and consistent description of energy and chemical feedback which should then produce realistic galactic outflows. An important advantage of the new scheme is that it avoids ad hoc scale-dependent parameters of the kind present in most previous work. This makes our scheme well suited to cosmological structure formation simulations where galaxies with a wide range of properties form simultaneously.

Our paper is organized as follows. In Section 2, we present the numerical implementations of our multiphase approach and of the energy feedback model, testing their performance using idealized simulations of disc galaxy formation. In Section 3, we use similar collapse simulations to discuss the impact of SN feedback on galaxy formation. We include an analysis of the effects on star formation and the generation of winds (Section 3.1), on chemical enrichment of the ISM and the IGM (Section 3.2), and within galaxies of differing total mass (Section 3.3). In Section 4, we analyse both such collapse simulations and simulations of equilibrium galaxies similar to the Milky Way, exploring whether a suitable choice of star formation efficiency allows us to reproduce the observed Kennicutt relation between the surface densities of gas and of star formation in galaxies. Finally, Section 5 summarizes our conclusions.

2 NUMERICAL IMPLEMENTATION

In this section, we discuss how we treat a multiphase ISM, and implement energy feedback from SN explosions. We also test the performance of these new numerical schemes, which are grafted

on to the version of GADGET-2 discussed in Paper I, which includes metal enrichment by Type II SNe (SNII) and Type Ia SNe (SNIa) as well as metal-dependent cooling.

2.1 Multiphase gas model

2.1.1 Model description

The ISM is known to have a complex, multiphase structure in which interpenetrating components of similar pressure but very different temperature and density span a wide range of spatial scales (e.g. McKee & Ostriker 1977; Efstathiou 2000). This multiphase character is difficult to represent appropriately in numerical simulations. In particular, standard implementations of SPH reproduce it poorly, because they have insufficient resolution to represent clouds of cool, dense gas embedded in a hotter diffuse medium. Numerical artefacts result from the SPH estimate of gas density which, in a commonly used implementation, can be written as

$$\langle \rho_i \rangle = \sum_j^N m_j W_{ij}, \tag{1}$$

where j runs through the N neighbours of particle i, m_j denotes the mass of particle j, and W_{ij} is a symmetrized kernel function. Diffuse phase particles close to a dense cloud overestimate their densities by including cloud particles in the sum over neighbours. This leads to an underestimation of their cooling times and so to excessive accretion of gas on to the cloud (Pearce et al. 1999). This then artificially boosts the star formation rate. A second, more serious problem, also caused by the lack of resolution, is that SN feedback is not channelled into the hot phase but rather is dumped in the dense gas surrounding star-forming regions, resulting in the immediate radiative loss of the energy and the confinement of the metals. This prevents the launching of galactic winds, the ejection of heavy elements, and the self-regulation of star formation activity.

In order to address these issues and to improve the treatment of the ISM in SPH, we have developed a multiphase scheme which allows a larger overlap of the diffuse and dense gaseous components and can be combined with a more effective scheme for injecting the energy and heavy elements from SNe. The innovation in our scheme relates to the selection of neighbours. If two gas particles have dissimilar thermodynamic properties, they are explicitly prevented from being neighbours in the SPH calculations. In detail, this works as follows. We *decouple* a given particle j from particle i, meaning that j is explicitly excluded from the neighbour list of i, if the following conditions are fulfilled:

$$A_i > \alpha A_j, \tag{2}$$

$$\mu_{ij} < c_{ij}, \tag{3}$$

where α is a constant, A_i is the entropic function of particle i, and μ_{ij}[1] and c_{ij} measure the pair-averaged local velocity divergence and sound speed, respectively. The entropic function characterizes the specific entropy s of gas particles through

$$P = A(s)\rho^\gamma, \tag{4}$$

where P denotes pressure and $\gamma = 5/3$ is the adiabatic index for a monatomic ideal gas. The second condition of equation (3) is included to avoid decoupling in shock waves, which, as noted by Marri & White (2003), can lead to unphysical effects when particles on opposite sides of a shock do not 'see' each other.

The code assumes a fixed mass within the smoothing length which corresponds to ∼32 neighbours (Springel & Hernquist 2003). In the context of our decoupling scheme, if the physical state of a given particle changes, a new list of neighbours is calculated to assure that the required ∼32 neighbours are enclosed.

Conservation of energy and momentum requires symmetric force evaluations between all particle pairs to ensure the validity of Newton's third law. Hence, for the force calculation only we include the extra requirement that if particle i excludes particle j from its neighbour list, then particle j does not consider particle i as a neighbour either. In this way the symmetry of force calculations is preserved in our code.

An important advantage of the above scheme is that the decoupling criterion is checked on a pair-wise basis. This allows a formulation which is independent of scale or resolution-dependent parameters. Only the dimensionless free parameter α needs to be set. A multiphase structure naturally appears in the gas component in this model once realistic cooling processes are included. This substantially improves the representation of the ISM in star-forming galaxies.

2.1.2 Tests of the model

In order to test the performance of this decoupling scheme, we carried out a set of idealized simulations of the formation of isolated disc galaxies similar to those in the early work of Navarro & White (1993). The initial conditions are generated by radially perturbing a spherical grid of superposed dark matter and gas particles to produce a cloud with density profile $\rho(r) \sim r^{-1}$ and radius $100\,h^{-1}$ kpc ($h = 0.7$). This sphere is initially in solid body rotation with an angular momentum characterized by spin parameter $\lambda \simeq 0.1$. The initial thermal energy of the system is only 5 per cent of its binding energy, i.e. the gas is cold. We have simulated a $10^{12}\,h^{-1}\,\mathrm{M}_\odot$ mass system, 10 per cent of which is in the form of baryons, and used ∼9000 particles for the gas and ∼9000 for the dark matter. This yields particle masses of $\sim 10^8\,h^{-1}\,\mathrm{M}_\odot$ for dark matter and $10^7\,h^{-1}\,\mathrm{M}_\odot$ for gas. We adopted gravitational softening lengths of 1.50 and $0.75\,h^{-1}$ kpc for dark matter and gas particles, respectively. In the tests presented in this section, we do not allow star formation, and the cooling assumed primordial element abundances.

We ran two simulations of the system described above, the only difference being the inclusion of our multiphase treatment. In the simulation including the multiphase model, we have adopted a decoupling parameter of $\alpha = 50$. In order to better highlight the effects of the multiphase model, we specify two reference phases, defined by $A \geqslant A_{\rm crit}$ for the 'hot' component, and $A < A_{\rm crit}$ for the 'cold' component, where $A_{\rm crit}$ is the entropic function corresponding to a temperature of $T = 2T_*$ and a density of $\rho = 0.1\rho_*$. Here $T_* = 4 \times 10^4$ K and $\rho_* = 7 \times 10^{-26}\,\mathrm{g\,cm^{-3}}$ are the star formation thresholds assumed in Paper I. We stress that these definitions are not related to the decoupling model and are only introduced to facilitate presentation of our results.

In the upper panel of Fig. 1 we compare the surface gas density profiles, projected on to the disc plane, of the two simulations after $0.9\,h^{-1}$ Gyr. Profiles for the 'hot' and 'cold' phases defined above are shown separately. In the lower panel, we plot the fraction of baryonic mass which is 'hot' as a function of radius. These plots have been made taking into account the gas within a vertical distance $|z| < 2\,h^{-1}$ kpc in order to restrict to the disc plane. The surface density

[1] We use the artificial viscosity term as parametrized in equation (14) of Springel (2005).

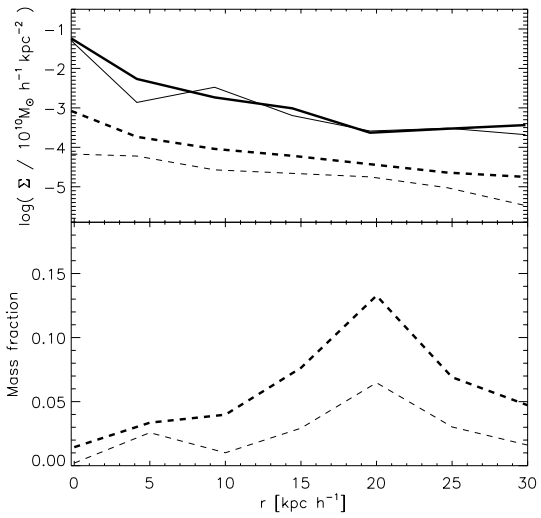

Figure 1. Top: surface density profiles projected on to the disc plane after $0.9\,h^{-1}$ Gyr for hot (dashed lines) and cold (solid lines) gas in our cooling-only simulations of isolated collapsing spheres carried out using a standard SPH implementation (thin lines) and using our decoupling scheme with $\alpha = 50$ (thick lines). Bottom: the fraction of baryonic mass belonging to the hot medium as a function of radius for the same two simulations. These plots are restricted to the disc plane with a vertical distance of $|z| < 2\,h^{-1}$ kpc.

profiles for the cold gas (solid lines) are almost indistinguishable, but the amount of hot gas (dashed lines) is greater at all radii when phase decoupling is included. From the lower panel we can see that the hot medium has grown at the expense of the cold one. This is a result of the elimination by the decoupling algorithm of the excess cooling discussed above.[2]

We have investigated the sensitivity of the decoupling scheme to the value of the free parameter α in equation (2). Too small a value for α would lead to decoupling of gas particles with very similar properties, while too large a value would produce no effect at all. We ran tests varying the value of α over the range $\alpha = 5$ to $\alpha = 100$, and found that our results are insensitive to the actual value within this range. This reflects the large entropy difference between the various phases of a realistic ISM caused by the structure of the radiative cooling function. We will generally choose $\alpha = 50$ for later experiments in this paper.

2.2 Energy feedback by SNe

2.2.1 Model description

Our model for energy feedback by SNe resorts to an explicit segregation of the gas surrounding a star particle into a cold dense phase and a diffuse phase, both for the release of SN energy and for the mixing of newly synthesized elements into the ISM. The separation into two phases, and the different treatment of them with respect to feedback, is motivated by previous attempts to model the release of SN energy, which have repeatedly found that this is ineffective if direct thermalization is invoked because the cold dense gas in which stars form has a very short cooling time (Katz 1992). In addition, the characteristic physical scales relevant to feedback in the real ISM are usually not resolved in galaxy formation simulations (Thacker & Couchman 2001).

Surrounding each star particle with exploding SNe we define two gaseous phases which we loosely denote *cold* and *hot*. The *cold* phase consists of gas with $T < 2T_*$ and $\rho > 0.1\rho_*$, while the rest of the gas is considered to be part of the *hot* phase, even though much of it may actually have $T < 2T_*$. These two phases are treated differently at the time of metal and energy distribution. The values of ρ_* and T_* (7×10^{-26} g cm^{-3} and 4×10^4 K, respectively) are typical of local star-forming regions and are assumed to be independent of the global properties of the systems. Note that these phases are not directly related to the decoupling scheme itself, or to the hot and cold gas components we used in the previous section to analyse some of our results.

In our approach, stars are assigned two different smoothing lengths, corresponding to the cold and hot phases. Both smoothing lengths are adjusted to enclose the same mass (we have assumed the mass corresponding to $\sim$32 neighbours). In the case of an extremely diffuse, hot phase, an unphysically large smoothing length could be required to enclose $\sim$32 neighbours. In order to avoid this behaviour, we set for each star particle a maximum length to search for hot neighbours, which we assumed to be 10 times the smoothing length calculated for its cold neighbours. We have tested the sensitivity of our results to this choice running simulations assuming different maximum lengths allowed ($\sim$10–100 times the cold smoothing length), finding that they are not affected. We stress the fact that the neighbour searches for stars have no relation to the SPH treatment for the gas.

Conceptually, we can divide our discussion of the SN energy feedback model into two main stages: energy production and energy release. We shall discuss them in turn.

To describe energy production, we have included the energy contributions associated with SNII and SNIa explosions. Briefly, our scheme works as follows: at each integration time-step, we calculate the number of SNII by adopting an initial mass function (IMF) and by assuming that stars more massive than $8\,\mathrm{M}_\odot$ end their lives as SNII after $\approx 10^6$ yr. For SNIa, we use the W7 model of Thielemann, Nomoto & Hashimoto (1993). In order to estimate the SNIa number, we adopt an observationally motivated relative rate with respect to SNII, and we assume a progenitor lifetime in the range [0.1, 1] Gyr as described in Paper I. Finally, we assume that each SN injects 10^{51} erg of energy into the surrounding gas.

In order to distribute the energy produced by a given star particle, we separately identify the gaseous neighbours that belong to the *hot* and to the *cold* phases. Smoothing lengths are calculated for the star particle so that the number of neighbours in each of these phases is similar to the number used in the SPH formalism to estimate hydrodynamical forces. Within each phase, gaseous neighbours then receive a fraction of the SN energy, weighted by the appropriate smoothing kernel.

We assume that a fraction ϵ_h of the SN energy is instantaneously thermalized and appears in the hot phase of the ISM around the star particle, while a fraction ϵ_r is directly radiated away by the cold phase. The remaining fraction of the energy, $\epsilon_\mathrm{c} = 1 - \epsilon_\mathrm{h} - \epsilon_\mathrm{r}$, is injected into the cold gas causing some of it to join the hot phase. Because there is no consensus on the phenomenology of the ISM which could provide specific values for these fractions, we assume them to be independent of local conditions and we treat them as free parameters to be adjusted so as to reproduce the observations of star-forming systems. We vary their values widely in order to analyse their impact on the dynamics of our model. Choosing $\epsilon_\mathrm{r} = 1$

[2] The entropy-conserving formulation of SPH (Springel & Hernquist 2002) implemented in GADGET-2 has solved the extreme problem of a near-absence of hot particles in the central regions found by Marri & White (2003) when carrying out a similar test using codes based on GADGET-1.

Table 1. Main properties of our simulations of idealized protogalaxy collapses. The columns give total mass, initial number of gas and dark matter particles, and the feedback input parameter (ϵ_c). We also list the final stellar mass fraction, the fraction of unbound baryons, the fraction of metals locked into the hot gas, and the fraction of metals locked into stars at $t = 1.0\,h^{-1}$ Gyr.

Test	$M_{\rm vir}(h^{-1}\,{\rm M}_\odot)$	$N_{\rm gas} = N_{\rm dark}$	ϵ_c	$M_{\rm star}/M_{\rm bar}$	$M_{\rm unbound}/M_{\rm bar}$	$f_{\rm met}^{\rm hot}$	$f_{\rm met}^{\rm stars}$
D12	10^{12}	9000	–	0.581	0.025	0.002	0.557
F12-0.1	10^{12}	9000	0.1	0.324	0.411	0.910	0.045
F12-0.5	10^{12}	9000	0.5	0.362	0.309	0.556	0.212
F12-0.9	10^{12}	9000	0.9	0.231	0.315	0.710	0.188
D11.5	$10^{11.5}$	9000	–	0.738	0.002	0.000	0.663
F11.5-0.1	$10^{11.5}$	9000	0.1	0.415	0.361	0.903	0.050
F11.5-0.5	$10^{11.5}$	9000	0.5	0.390	0.441	0.755	0.170
F11.5-0.9	$10^{11.5}$	9000	0.9	0.276	0.613	0.793	0.152
D11	10^{11}	9000	–	0.824	0.000	0.000	0.703
F11-0.1	10^{11}	9000	0.1	0.398	0.364	0.904	0.044
F11-0.5	10^{11}	9000	0.5	0.403	0.407	0.694	0.169
F11-0.9	10^{11}	9000	0.9	0.273	0.666	0.813	0.146
D10.5	$10^{10.5}$	9000	–	0.712	0.000	0.000	0.608
F10.5-0.1	$10^{10.5}$	9000	0.1	0.342	0.416	0.903	0.043
F10.5-0.5	$10^{10.5}$	9000	0.5	0.318	0.525	0.780	0.141
F10.5-0.9	$10^{10.5}$	9000	0.9	0.207	0.779	0.881	0.119
D10	10^{10}	9000	–	0.520	0.000	0.000	0.426
F10-0.1	10^{10}	9000	0.1	0.271	0.501	0.911	0.031
F10-0.5	10^{10}	9000	0.5	0.258	0.633	0.848	0.107
F10-0.9	10^{10}	9000	0.9	0.174	0.819	0.901	0.085
D9.5	$10^{9.5}$	9000	–	0.451	0.000	0.000	0.405
F9.5-0.1	$10^{9.5}$	9000	0.1	0.155	0.548	0.913	0.017
F9.5-0.5	$10^{9.5}$	9000	0.5	0.184	0.821	0.899	0.101
F9.5-0.1	$10^{9.5}$	9000	0.9	0.113	0.902	0.945	0.051
D9	10^{9}	9000	–	0.373	0.004	0.000	0.382
F9-0.1	10^{9}	9000	0.1	0.107	0.596	0.912	0.011
F9-0.5	10^{9}	9000	0.5	0.041	0.662	0.840	0.031
F9-0.9	10^{9}	9000	0.9	0.069	0.927	0.950	0.044
F12-0.5-H	10^{12}	40000	0.5	0.365	0.386	0.735	0.204
F10-0.5-H	10^{10}	40000	0.5	0.240	0.326	0.782	0.095
F9-0.5-H	10^{9}	40000	0.5	0.061	0.924	0.954	0.036

implies that all the SN energy is radiated away by the cold phase with no impact on the overall dynamics. Examples of the evolution in this extreme case are given by our multiphase-only runs (e.g. D12 in Table 1). For the sake of simplicity, we have chosen $\epsilon_r = 0$ in the rest of our tests, noting that a non-zero value could always be compensated by a different IMF or different assumed SN energies. In this case, the effects of feedback depend only on ϵ_h (or ϵ_c). In practice, both ϵ_h and ϵ_r should be varied in order to get the best possible match to observation.

For each gas particle belonging to the cold phase, we define a *reservoir* in which the SN energy that the particle receives from successive SN explosions is accumulated. Once the accumulated energy ($E_{\rm res}$) is high enough to modify the thermodynamic properties of a cold gas particle in such a way that its new properties will resemble those of the hot phase, we *promote* the cold particle, dumping its reservoir energy into its internal energy. This *promotion scheme* has been developed in order to prevent artificial losses of the SN energy by the cold phase and to ensure that cold ISM gas can be entrained in outflows, producing *mass-loaded* galactic winds.

In order to decide whether the promotion of a given cold particle should take place, we consider the following physical conditions: (i) the final physical state we want the particle to reach and (ii) the energy needed for the process to take place, given its current physical state. Since we want to mimic the transformation of cold gas into gas that is in thermal equilibrium with the hot-gas surroundings, we require that the final state for a cold particle that is promoted should be similar to that of its local hot phase environment. Based on our decoupling scheme, the local hot phase of any given cold gas particle is naturally defined by those neighbours from which the cold particle is decoupled (see Section 2.1).

Assuming that the transformation from the cold to the hot phase takes place at constant pressure, we define a *promotion energy* for each particle. This promotion energy ($E_{\rm prom}$) takes into account the energy needed not only to raise the temperature of the particle to that of its hot neighbours, but also for it to expand against the ambient

pressure to reach their mean density.[3] Thus, we require the promoted particle to have an entropic function at least as high as the mean of those of its hot neighbours ($A^{\rm hot}_{\rm Avg}$). The conditions for promotion are the following:

$$E_{\rm res} > E_{\rm prom} = \frac{\gamma}{\gamma - 1}\, m_i \left[A^{\rm hot}_{\rm Avg}\, (\rho^{\rm hot}_{\rm Avg})^{\gamma-1} - A_i\, \rho_i^{\gamma-1} \right], \quad (5)$$

$$A_{\rm new} > A^{\rm hot}_{\rm Avg}. \quad (6)$$

Here, $A_{\rm new}$ is an estimate of the new entropic function of the particle after promotion and $A^{\rm hot}_{\rm Avg}$ and $\rho^{\rm hot}_{\rm Avg}$ are the mean entropic function and mean density of the hot neighbours surrounding the cold gas particle, respectively. The value of $A_{\rm new}$ is calculated assuming that the energy of the particle after promotion will be its actual energy plus the reservoir and that the new density will be the average density of the hot neighbours, $A^{\rm hot}_{\rm Avg}$.

This scheme guarantees that once a gas particle is promoted, it will have thermodynamic properties matching those of its local hot environment. Consequently, it will remain hot at least as long as nearby hot material. The procedure also ensures that the smooth character of SPH is preserved and no 'flip-flop' instabilities are generated during promotion. Note that the promotion criterion is evaluated for each cold gas particle individually, and that it depends both on the particle's own thermodynamic properties and on those of its local hot environment. This scheme allows us to mimic the reheating of cold interstellar gas by SN explosions, providing a link between SN energy feedback and our multiphase treatment, and resulting in a self-regulated star formation cycle.

We also include an extra requirement for promotion in order to treat cases where cold particles have few hot neighbours within the maximum smoothing length allowed, for example because all gas is cold. If this happens, we prefer to keep the particle in the cold phase until a well-defined hot environment has formed. This ensures numerical stability in cases where the hot phase does not exist or is very poorly sampled. We consider the hot environment to be well defined if it is numerically resolved. We therefore require a minimum of hot neighbours to be identified before a cold particle to be eligible for promotion. We have run simulations with different choices and find that at least five hot neighbours are needed to avoid instabilities and to get converged results. In the experiments presented in this paper, we adopt this minimum number.

In the case where a cold gas particle satisfies the conditions to be transformed into a star particle when still having a reservoir of energy, we distribute this energy to its cold-phase neighbours using the smoothing kernel. In the extreme case that there are no cold neighbours, the energy is assumed to be lost and the reservoir is reset to zero. Finally, a numerical artefact could also develop in our scheme when cold particles become 'hot' by numerical noise (near the density and temperature thresholds segregating phases). In this case, the SN energy is immediately thermalized and the reservoir is reset to zero. If this happens, feedback energy is often lost because these particles immediately radiate the newly thermalized energy. We have checked, however, that averaged over a simulation's duration the total reservoir energy lost in this way is a negligible fraction ($\sim 10^{-5}$) of the total energy produced by SN.

[3] The internal energy of a particle i is described as $U_i = (\gamma - 1)^{-1}\, m_i A_i\, \rho_i^{\gamma-1}$. Since we consider a process at constant pressure, we need energy not only to raise the temperature of the particle but also to work against the background pressure as it expands. Expressed differently: $\mathrm{d}Q = \mathrm{d}U + P\,\mathrm{d}V$ with $P\,\mathrm{d}V = (\gamma - 1)\,\mathrm{d}U$, which results in equation (5).

Finally, we have also slightly modified the chemical enrichment model of Paper I to work in a consistent fashion with our new treatment of the SN energy. To this end, we distribute the chemical elements into the hot and cold phases of a given star particle similarly to the energy distribution. For metal distribution we assume different fractions $\epsilon^m_{\rm c}$ and $\epsilon^m_{\rm h}$ so that $\epsilon^m_{\rm c} + \epsilon^m_{\rm h} = 1$. These fractions could, in principle, be tuned differently than the fractions for energy distribution in order to match observations. Our model assumes that the chemical distribution always occurs simultaneously with SN explosions, i.e. there is no metal reservoir corresponding to the promotion scheme described above. Clearly, it would be possible to choose different fractions for distributing heavy elements than for distributing energy but, at this stage, we prefer to avoid additional parameters by assuming the metal fractions to be equal to the energy fractions in all experiments analysed in this paper.

2.2.2 *Tests of the model*

As a first test of the dynamics of our numerical scheme, we have run a set of simulations of the evolution of the idealized initial conditions described in Section 2.1. These experiments include metal-dependent radiative cooling, star formation, chemical enrichment and energy feedback. They have all been run with the same star formation and chemical input parameters: a star formation efficiency $c = 0.1$, a Salpeter IMF with lower and upper mass cut-offs of 0.1 and 40 $\mathrm{M}_\odot$, respectively, a SNIa rate of 0.3 relative to SNII which is a typical value coming from observations in Sa–Sb galaxies (as used in Paper I), and a lifetime interval of [0.1, 1] Gyr for SNIa (see Paper I for details). We have assumed an instantaneous recycling approximation for SNII. We have used metal-dependent cooling functions adapted from Sutherland & Dopita (1993) as described in Paper I, and assume no cooling for gas particles with temperature lower than 10^4 K. The decoupling scheme has been turned on for all the experiments with a decoupling parameter of $\alpha = 50$. We have used gravitational softening lengths of 1.50, 0.75 and 1.13 h^{-1} kpc for dark matter, gas and star particles, respectively.

We here analyse simulations of systems of different mass, run with feedback parameter $\epsilon_{\rm c} = 0.5$. For comparison, we have computed corresponding reference simulations without SN feedback in all cases. Three higher resolution simulations have also been done to test numerical convergence. For the different total masses, the softening lengths as well as the initial radii have been scaled in proportion to $M^{1/3}$, relative to the parameters assumed for the $10^{12}\, h^{-1}\, \mathrm{M}_\odot$ system, leading to identical collapse times and characteristic densities for all systems. The main properties of these simulations are summarized in Table 1.

In order to assess how the energy feedback model and the promotion scheme work, we show in Fig. 2 the effects of promotion on individual particles. As explained earlier, each cold gas particle has been assigned a reservoir in which we keep track of the energy it receives from nearby SN explosions. This reservoir energy is accumulated until the particle is eventually promoted, dumping its reservoir into its internal energy. In Fig. 2, we plot the properties of promoted particles in a density-temperature plot for our test F12-0.5. The arrows point from the original location of each cold gas particle to its new position after promotion, and the different panels correspond to particles promoted in different time intervals. It is clear that our feedback model is successful in driving a gas flow from the cold, dense phase into the hot, diffuse medium where the promoted particles share the properties of their local hot environment. Note that the hot environment evolves with time, and consequently, the

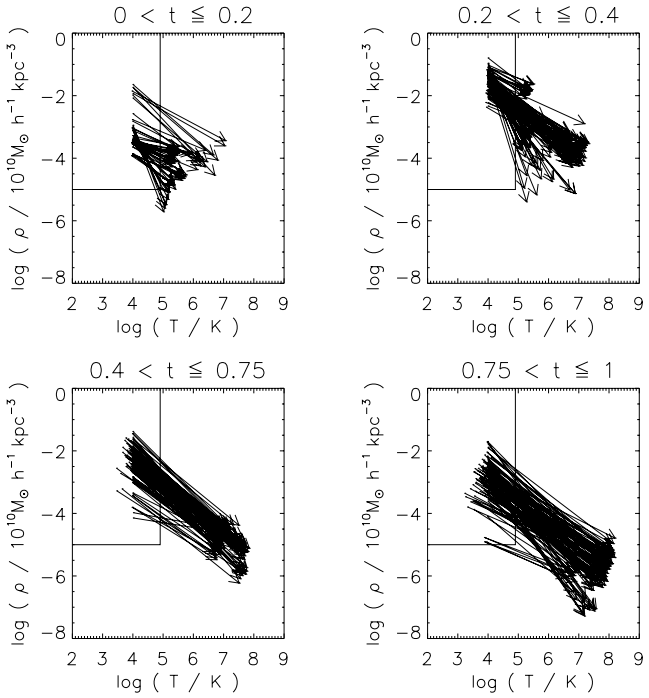

Figure 2. Temperature–density distribution of promoted particles in F12-0.5, which corresponds to a $10^{12}\,h^{-1}\,\mathrm{M}_{\odot}$ mass system, run with energy feedback and $\epsilon_{\mathrm{c}} = 0.5$. The arrows point from the initial state before promotion to the final one after promotion. The solid lines separate the cold and hot phases of the feedback scheme. The different panels correspond to particles promoted in different time intervals, indicated in units of h^{-1} Gyr.

new location of promoted particles on the temperature–density plot changes accordingly. This flexibility arises because we do not prescribe in advance the thermodynamic properties of the hot and cold phases.

A further consequence of the reheating of cold gas and its promotion into the hot phase is the generation of a significant outflow of material from the system. As an illustrative example, we show in Fig. 3 an edge-on projection of the velocity field of promoted particles (arrows) in F12-0.5. Different panels correspond to different times during the evolution of the system: $t = 0.3$ (upper left-hand panel), 0.4 (upper right-hand panel), 0.75 (lower left-hand panel) and $t = 1.0\,h^{-1}$ Gyr (lower right-hand panel). In each panel, the velocity field has been calculated using particles promoted in the last $0.2\,h^{-1}$ Gyr. The lengths of the arrows scale with the magnitude of the local velocity, with the longest arrows corresponding to $\sim$1000 km s^{-1}. The background colour represents the projected metallicity for the total gas component. From this figure we can see that our promotion scheme establishes an effective mechanism for transporting gas from the centre of the discs into the haloes. Once particles are promoted, they are accelerated outwards, moving mainly in the direction perpendicular to the disc plane. As may be seen from this figure, the outflow is not completely symmetric, since it is determined by the local geometry of the gas and the stellar distribution. Note that the inclusion of energy feedback allows us to account for chemical enrichment of the region outside the discs since the galactic outflows are able to transport a significant fraction of the heavy elements (defined as all chemical elements higher than hydrogen and helium) outwards. We will come back to the impact of SN energy feedback on the chemical properties of galaxies in Section 3.2.

The exchange of mass between the cold and hot phases driven by our promotion scheme strongly affects the evolution of the systems and their resulting mass distributions. In Fig. 4, we show face-on projections of the discs in D12 (no energy feedback; upper panels) and F12-0.5 (with energy feedback; lower panels) at $t = 1.2\,h^{-1}$ Gyr. We show the hot and cold media defined in Section 2.1 separately, as well as the stellar component. We can see from this figure that energy feedback helps to generate a well-defined hot phase which is distributed out to $\sim 300\,h^{-1}$ kpc in this particular experiment. In the case of no energy feedback (upper panels) the hot phase is produced only by the collapse and virialization of the system, is a small fraction of the gaseous mass, and remains bound within $\sim 100\,h^{-1}$ kpc. In this latter case, most of the gas has been able to cool and condense, producing a large stellar clump in the centre.

We have also tested how numerical resolution affects the evolution of systems of different total mass. For this purpose we ran three additional simulations increasing the initial number of gas and dark matter particles up to 40 000 in each mass component (see Table 1). These tests were performed for systems with total masses of 10^{9}, 10^{10} and $10^{12}\,h^{-1}\,\mathrm{M}_{\odot}$ (F12-0.5-H, F10-0.5-H, F9-0.5-H, respectively) using a feedback parameter of $\epsilon_{\mathrm{c}} = 0.5$ in all cases. In Fig. 5, we show the evolution of the star formation rate for these models and compare them with their lower resolution counterparts. From this figure we can see that the results are reasonably well converged for the higher halo masses. For the smallest system, stochastic bursting behaviour is observed so convergence is difficult to test.

3 ANALYSIS AND RESULTS

In this section, we analyse the effects of our new feedback scheme on simulations of galaxy formation. In particular, we test the dependence of our results on the adopted feedback parameters, and we investigate the impact of the energy feedback on the resulting metal distributions. We also discuss the dependence of the results on the total system mass.

3.1 Star formation and outflows

In order to assess the response of galaxies to the adopted feedback parameters, we compare simulations F12-0.1, F12-0.5 and F12-0.9 (see Table 1) which only differ in the adopted value of ϵ_{c}. In Fig. 6, we show the evolution of the cold ($A < A_{\mathrm{crit}}$, upper panel) and hot ($A \geqslant A_{\mathrm{crit}}$, middle panel) gaseous mass, in units of the total baryonic mass. For comparison, we also include the corresponding relations for simulation D12 which was run without energy feedback.

We have also estimated the fraction of unbound gas (lower panel), defining it here as the gas with a positive sum of kinetic and gravitational potential energy. As can be seen from this figure, the simulations with energy feedback have larger fractions of hot and unbound gas compared with their counterpart D12, indicating that the gas has been both heated and accelerated outwards. Note, however, that the effect of varying the input parameter ϵ_{c} is not simple. This is a consequence of the non-trivial interplay between release of SN energy, promotion from cold to hot gas, and radiative cooling. All these processes influence the gas accretion and star formation rates and the formation of the cold and hot phases. As reference values we give in Table 1 the unbound gas fraction for all test simulations after $1.0\,h^{-1}$ Gyr of evolution.

As a consequence of the exchange of material between the phases, our scheme can effectively regulate star formation activity. This can be appreciated from Fig. 7 where we show star formation rate

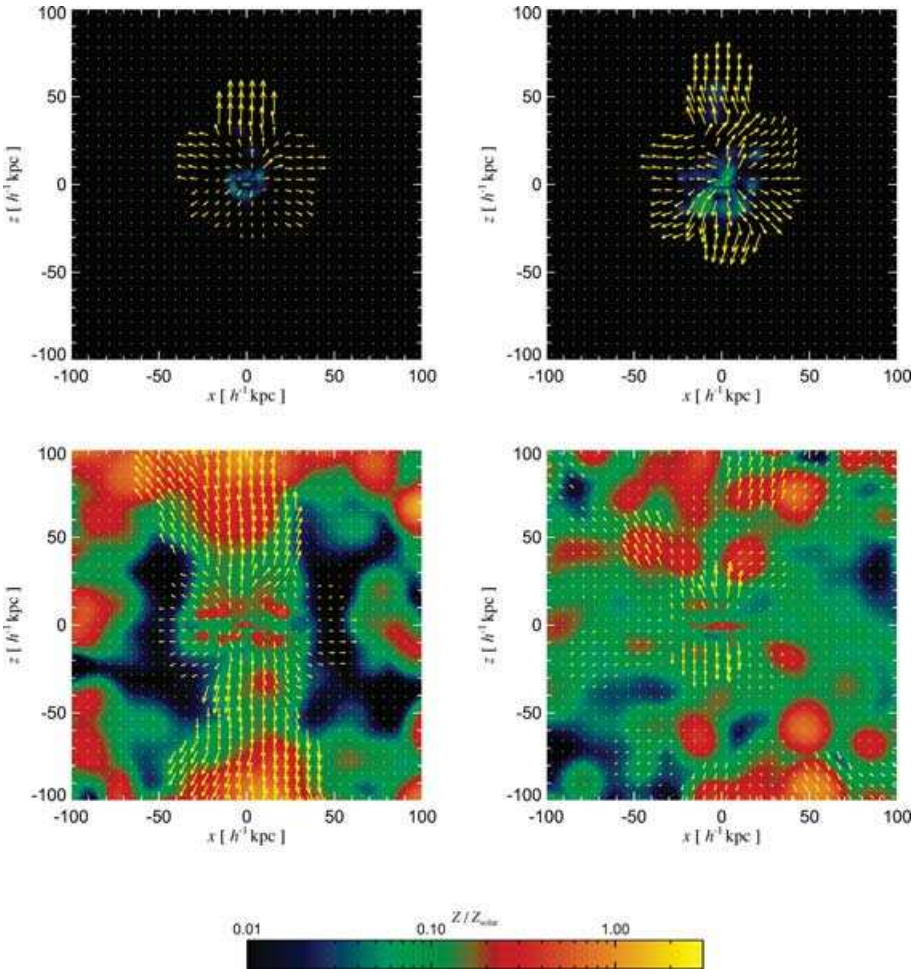

Figure 3. Projected velocity field of recently promoted particles (i.e. particles promoted in the last $0.2\,h^{-1}$ Gyr, arrows) for our simulation F12-0.5 with SN feedback with $\epsilon_{\rm c} = \epsilon_{\rm h} = 0.5$. The different panels correspond to different times in the evolution of the system: $t = 0.3$ (upper left-hand panel), 0.4 (upper right-hand panel), 0.75 (lower left-hand panel) and $1.0\,h^{-1}$ Gyr (lower right-hand panel). The lengths of the arrows scale with the magnitude of the local velocity, with the longest arrows corresponding to $\sim$1000 km s^{-1}. The colour map in the background encodes the projected metallicity field, according to the colour-scale shown at the bottom.

and integrated stellar mass fraction as a function of time for our simulation series. Note that for the initial conditions adopted here, particles initially located at the edge of the system fall to the centre at $t \approx 0.55\,h^{-1}$ Gyr. Compared to D12, SN feedback reduces the final stellar mass by $\sim$45, 40 and 65 per cent for F12-0.1, F12-0.5 and F12-0.9, respectively (see also Table 1). The larger $\epsilon_{\rm c}$, the more energy injected into the cold phase, the sooner promotion becomes significant, leading to a reduction in the amount of cold gas and the suppression of star formation. On the other hand, as $\epsilon_{\rm c}$ increases, less energy is dumped into the hot phase, making it easier both for hot gas to cool on to the disc and for cold gas to be promoted. The interplay between these processes leads to a non-monotonic dependence of the overall star formation efficiency on $\epsilon_{\rm c}$.

Since in these tests promoted particles define the outflows, we show in Fig. 8 the mass fraction in promoted gas as a function of z-velocity $v_{\rm z}$, defined as positive if particles are moving away from the centre and negative otherwise. Results are given for F12-0.1, F12-0.5 and F12-0.9 after $0.8\,h^{-1}$ Gyr of evolution (just after the maximum in star formation activity). For our test without SN energy feedback (D12), we calculated that 89 per cent of the gaseous mass has $|v_{\rm z}| < 100$ km s^{-1}, with an upper limit of $|v_{\rm z}| \approx 500$ km s^{-1}. In contrast, as may be seen in Fig. 8, in our simulations with feedback the fraction of *promoted* gas with $v_{\rm z} > 500$ km s^{-1} varies from 22 to 64 per cent. Clearly our scheme can produce outflows with relatively high velocities; the upper limits have increased to $v_{\rm z} > 1000$ km s^{-1}. We can also infer from this figure that the fraction of promoted gas which flows back into the system (indicated by negative velocities) is small. Observationally, the velocities associated with galactic outflows are found to vary from a few hundred to thousands of kilometres per second (e.g. Lehnert & Heckman 1995, 1996). Here, we do not intend to make a detailed comparison with observations but to investigate the typical z-velocities that the gas components associated with outflows may reach in our model. Our estimates show that the simulated outflows can reach z-velocities in the observed range. Note, however, that the correspondence between the observed line shifts and the velocities we measure in our simulations is not straightforward because of the variety of hydrodynamical, ionization and radiative transfer processes occurring in real systems.

3.2 Metal distribution

The redistribution of the gas owing to the injection of energy by SNe also affects the chemical abundances of the cold and hot gas

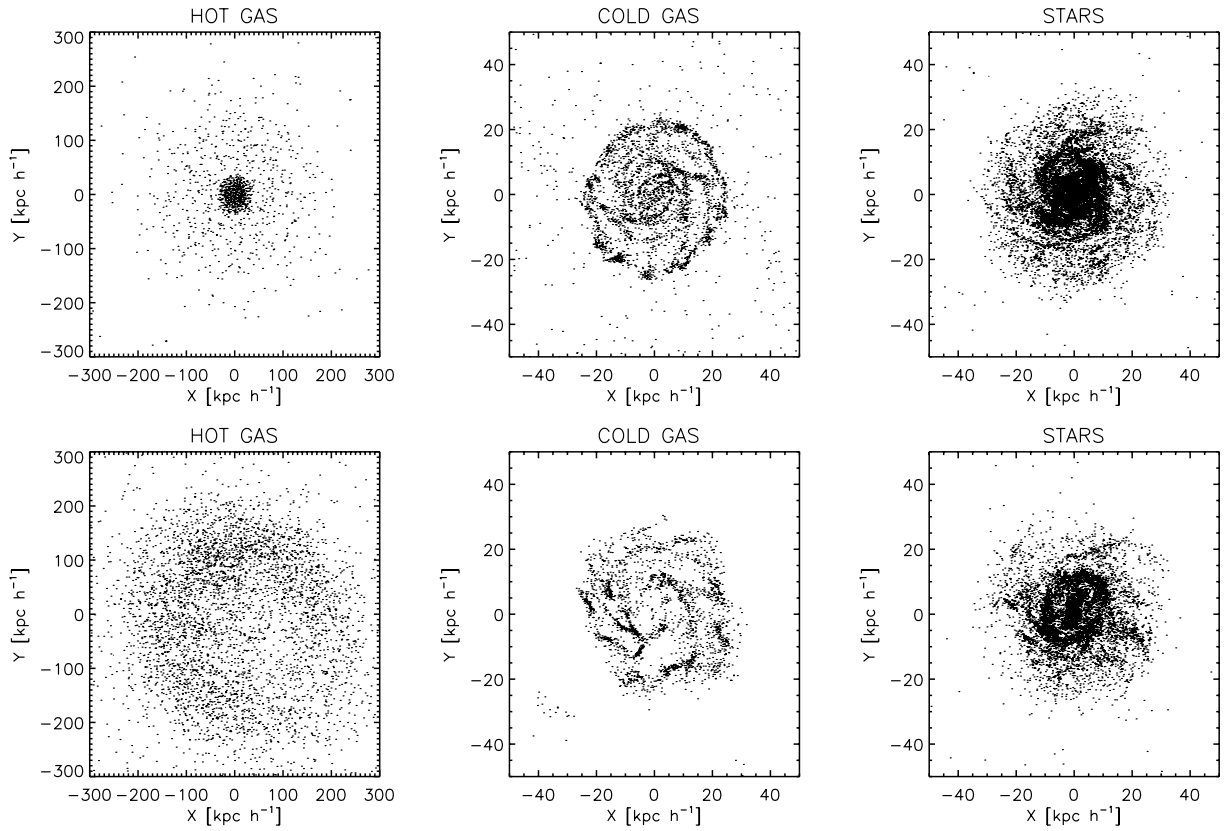

Figure 4. Face-on projections of the discs in $10^{12}\,h^{-1}\,\mathrm{M}_{\odot}$ systems after $1.2\,h^{-1}$ Gyr of evolution. We show the hot gas ($A \geqslant A_{\rm crit}$), the cold gas ($A < A_{\rm crit}$) and the stars separately, both for D12 (no energy feedback; upper panels) and for F12-0.5 (SN feedback with $\epsilon_{\rm c} = \epsilon_{\rm h} = 0.5$; lower panels).

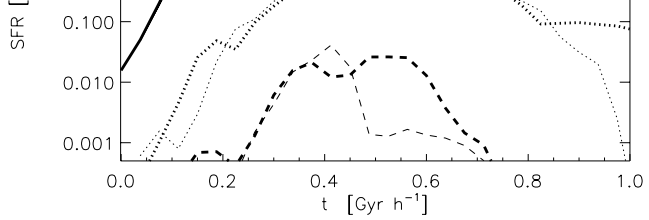

Figure 5. Star formation rates for F12-0.5 (solid thin line), F12-0.5-H (solid thick line), F10-0.5 (dotted thin line), F10-0.5-H (dotted thick line), F9-0.5 (dashed thin line) and F9-0.5-H (dashed thick line), corresponding to idealized protogalactic collapses of differing total mass and numerical resolution.

and those of the stars. It is thought that SN feedback could be the mechanism responsible for the transport of heavy elements into the intergalactic medium. In order to study this process in detail, it would be necessary to simulate galaxies in their correct cosmological setting, which goes beyond the scope of this paper. As a first step, we can however investigate the potential effects of our feedback model on the metal distribution using our idealized simulations of protogalactic collapses of total mass $10^{12}\,h^{-1}\,\mathrm{M}_{\odot}$ (see Table 1).

In Fig. 9 (left-hand panels), we show the evolution of the fraction of metals locked into cold gas ($A < A_{\rm crit}$), hot gas ($A \geqslant A_{\rm crit}$) and stars, normalized to the final total mass in heavy elements, for D12, F12-0.1, F12-0.5 and F12-0.9. In the right-hand panels of Fig. 9, we also display the mean metallicity Z, in units of solar metallicity, for these same simulations. Note that the total mass in metals in the system is a function of time owing to ongoing star formation. From this figure we can see that if energy feedback is not included, the metal content remains completely locked into the stellar and cold gas components. This is expected, since there is no efficient mechanism to transport metals away from the star-forming ISM. This situation is radically changed by the powerful winds generated by the SN feedback scheme. These outflows redistribute the metals, increasing the amount of enriched hot gas at the expense of the cold gas and stars. Note that even in F12-0.9, for which only 10 per cent of the metals are directly injected into the hot phase, the dynamical and thermal evolution of the system differs markedly from the case without energy feedback, showing efficient enrichment of the hot gas. This is driven by promoted material which was enriched while cold. In the case of F12-0.1, the cold gas and the stars end up with a negligible fraction of the metals. These trends are also reflected in the mean metallicities of the gaseous and stellar components. Fine-tuning $\epsilon_{\rm c}$ and $\epsilon_{\rm r}$ in a simulation with self-consistent cosmological initial conditions may allow one to reproduce the observed metallicity trends for hot gas, cold gas and stars. We will attempt this for a Milky Way look-alike in a forthcoming paper.

3.3 Dependence on virial mass

From a theoretical point of view, SN feedback is expected to play a crucial role in regulating the star formation activity in galaxies and in determining the level of enrichment of different environments.

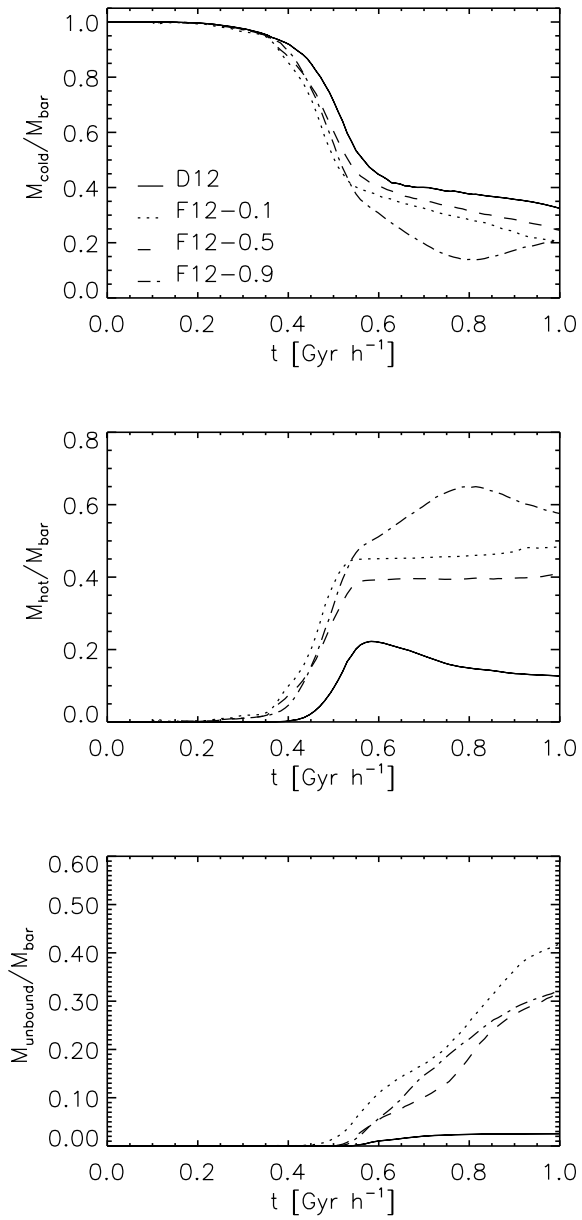

Figure 6. Evolution of the mass fraction in cold gas ($A < A_{\rm crit}$), hot gas ($A \geqslant A_{\rm crit}$) and unbound gas, normalized to the total baryonic mass of the system for simulations D12 (no energy feedback) and F12-0.1, F12-0.5 and F12-0.9 (with energy feedback but with different $\epsilon_{\rm c}$ values).

It is also expected that the impact of SN feedback should depend strongly on virial mass, where smaller mass systems should be more strongly affected, their shallower gravitational potential wells making it easier for the SNe to drive outflows (Larson 1976; White & Rees 1978; Dekel & Silk 1986). This concept has been widely applied in semi-analytic models of galaxy formation to explain several basic observational properties of the galaxy population such as the faint-end slope of the luminosity function (e.g. White & Frenk 1991). In previous sections, we have demonstrated that our energy feedback model is able to produce gas outflows which lead to different levels of enrichment, depending on the adopted $\epsilon_{\rm c}$ value. In this section, we discuss the effects of SN energy feedback as a function of the mass of the systems considered.

We again start from our idealized spherical initial conditions for protogalactic collapse. These initial conditions are simple enough to highlight the effects of feedback without being distracted by additional processes such as mergers and infall, which complicate the picture in fully hierarchical scenarios for galaxy formation. We analyse results from simulations that cover the total mass range 10^9–$10^{12}\,h^{-1}\,{\rm M}_\odot$, as well as different choices of the feedback parameters (see Table 1). For comparison, we have also analysed simulations without feedback.

Fig. 10 compares star formation histories for systems of differing total mass, in each case for simulations without SN energy feedback (solid lines) and with the feedback model enabled, using $\epsilon_{\rm c} = 0.1$ (dotted lines), $\epsilon_{\rm c} = 0.5$ (dashed lines) and $\epsilon_{\rm c} = 0.9$ (dashed–dotted lines). Clearly, SN feedback has a strong impact on these systems regardless of their total mass. For larger masses, the primary effect of SN feedback is a decrease in star formation activity. As one moves to lower mass systems, SN feedback modifies the star formation rates not only by decreasing the overall level of activity, but also by changing their character, producing a series of starbursts. From Fig. 10, we can also infer that increasing the value of $\epsilon_{\rm c}$ generally leads to stronger feedback effects at all times. In particular, larger $\epsilon_{\rm c}$ values are able to trigger several starburst episodes and to produce a significant decrease in the star formation activity at later times. Note that, specially for the smallest galaxies, star formation can stop completely after $\sim 1\,h^{-1}$ Gyr because the systems can lose their gas reservoirs. However, if more realistic initial conditions were considered, gas accretion from the intergalactic medium could contribute to fuel new star formation activity at later times.

The results obtained for our smallest virial masses, in which the star formation histories show episodic, bursty behaviours, are consistent with observational studies of dwarf galaxies (e.g. Kauffmann et al. 2003; Tolstoy et al. 2003). Numerical simulations assuming different types of initial conditions have also found such bursty behaviour for the star formation activity in small mass systems (e.g. Steinmetz & Navarro 1999; Carraro et al. 2001; Mayer et al. 2001; Pearce et al. 2001; Chiosi & Carraro 2002; Springel & Hernquist 2003). Some of these papers assume CDM universes in which star formation is mainly triggered by mergers, while others assume galaxies to form by monolithic collapse of baryons inside virialized dark matter haloes. Although most of them have considered the effects of SN feedback, none has succeeded in establishing a self-regulated star formation activity without introducing scale-dependent parameters.

In Fig. 11, we show the fraction of unbound gas as a function of virial mass after $0.85\,h^{-1}$ Gyr of evolution, for simulations with $\epsilon_{\rm c} = 0.1$ (dotted line), $\epsilon_{\rm c} = 0.5$ (dashed line) and $\epsilon_{\rm c} = 0.9$ (dashed–dotted line). We also show the results for our higher resolution simulations with $\epsilon_{\rm c} = 0.5$ (squared asterisks). As discussed earlier, the unbound gas fraction can be viewed as a proxy for feedback strength since it quantifies the fraction of baryons that are swept away from the system as a result of a feedback-driven outflows. For a given total mass, as the value of $\epsilon_{\rm c}$ is increased, the fraction of unbound gas increases. If no feedback is included, the fraction of unbound gas is negligible. As expected, for a given value of $\epsilon_{\rm c}$, SN feedback has stronger effects as we go to smaller systems. The smaller the system, the larger the fraction of unbound gaseous mass and the smaller the final stellar mass fraction (see Table 1). These trends with total mass are very encouraging, suggesting that our feedback model may reproduce the shape of the faint end of the galaxy luminosity function in hierarchical clustering scenarios (e.g. Trentham & Tully 2002). This has been an elusive goal in high-resolution simulations of galaxy formation thus far. The self-consistent regulation of the star formation activity together with the natural production of vigorous

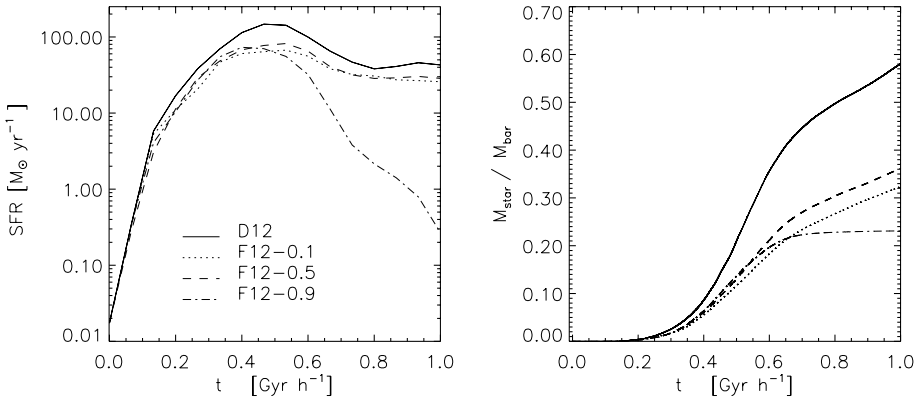

Figure 7. Evolution of the star formation rate (left-hand panel) and integrated stellar mass fraction (right-hand panel) for D12 (no energy feedback), and F12-0.1, F12-0.5 and F12-0.9 (SN energy feedback with different values of ϵ_c).

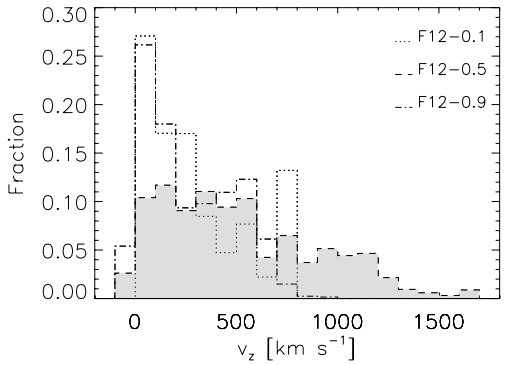

Figure 8. Fraction of promoted gas mass as a function of z-velocity, defined here as positive if particles are flowing away from the centre and negative otherwise. The plot shows results for our simulations of the $10^{12}\,h^{-1}\,M_\odot$ system, run with different feedback parameters: F12-0.1 (dotted lines), F12-0.5 (dashed lines) and F12-0.9 (dotted–dashed lines), at time $t = 0.8\,h^{-1}$ Gyr of the evolution.

outflows can be viewed as an important achievement of our new feedback model.

Finally, in Fig. 12 we show the fraction of metals locked into the unbound gas (thin lines) and into the stellar component (thick lines), as a function of total mass after $0.85\,h^{-1}$ Gyr. We show the results for simulations with $\epsilon_c = 0.1$ (dotted line), $\epsilon_c = 0.5$ (dashed line) and $\epsilon_c = 0.9$ (dashed–dotted line) and for our higher resolution tests with $\epsilon_c = 0.5$ (squared asterisks). From this figure we can see that the unbound gas is highly enriched, even in the largest mass systems. The anticorrelation in this figure indicates that the fraction of metals locked into the unbound gas increases with decreasing total mass. In contrast, the fraction of metals locked into stars increases slightly with the virial mass. In this case, note that the fraction of metals locked into the stellar component is less than 20 per cent which is perhaps suggestive of the need for a top-heavy IMF (Nagashima et al. 2005). This could help to reach higher abundances for the stellar populations, in better agreement with observation (e.g. Gallazzi et al. 2005). Also note that in the simulations with $\epsilon_c = 0.1$, most of the metal content of the system is located in the unbound gas.

The above results suggest that smaller systems would contribute to the enrichment of the intergalactic medium with larger fractions of their metal production. However, as large systems also produce important fractions of unbound and enriched gas, the amount of metals they release into the intergalactic medium could be very significant or even dominant. This behaviour may explain recent observational findings on the stellar mass–metallicity relation (Tremonti et al. 2004) where fewer metals were detected in massive galaxies than expected for closed box models, demonstrating rather directly that galaxies of all masses may have lost heavy elements to their surroundings.

The dependence of the impact of SN energy input on galaxy escape velocity may be able to explain the observed mass–metallicity relation in the context of a ΛCDM universe (e.g. De Lucia, Kauffmann & White 2004). Using the chemically enhanced GADGET-2 of Paper I (but without our new feedback scheme), Tissera, De Rossi & Scannapieco (2005) found that in the absence of strong winds a mass–metallicity relation is produced which is less steep at low masses than that observed (e.g. Tremonti et al. 2004). In future work, we will explore the mass–metallicity relation of galaxies in full cosmological simulations using our new SN energy feedback model.

4 STAR FORMATION EFFICIENCY AND THE KENNICUTT LAW

Our decoupling, star formation and feedback schemes contain a number of numerical and physical parameters for which values must be chosen. We discussed the phase separation parameters α, T_* and ρ_* in Sections 2.1 and 2.2, arguing that the behaviour of our algorithms is not sensitive to their precise values; α is chosen to achieve effective decoupling of gas at very different entropies while the values of density and temperature which define cold gas for the purpose of our feedback algorithms are based on the shape of the radiative cooling curve and the properties of observed star-forming regions. In addition, values must be chosen for the efficiencies of star formation and of energy deposition in hot and cold gas, for the chemical yields from stellar evolution, and for parameters which regulate the distribution of metals between the gas components. In previous sections we explored the effects of varying the efficiencies with which energy is deposited in hot and cold gas and we tied the distribution of metals to that of energy. In this section, we determine appropriate values for the star formation efficiency.

Observationally, it is found that star formation rate per unit area is remarkably tightly correlated with total gas surface density (Kennicutt 1998). This purely empirical relation holds as a function of radius within galaxies as well as among galaxies of very different mass, type and redshift. It is a considerable challenge for galaxy formation models such as our own to reproduce this

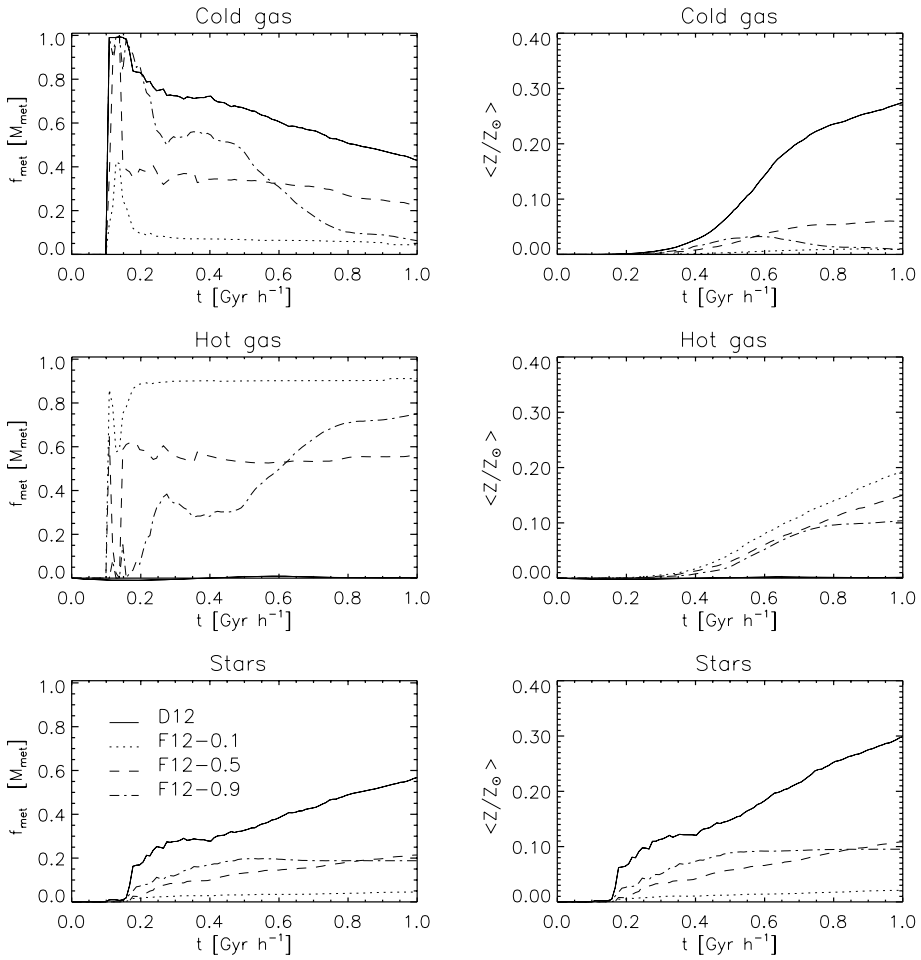

Figure 9. Evolution of the fraction of metals in the cold gas ($A < A_{\rm crit}$), hot gas ($A \geqslant A_{\rm crit}$) and in the stars (left-hand panels), for our $10^{12}\,h^{-1}\,{\rm M}_{\odot}$ mass system. We show results for simulation D12 without energy feedback, and for simulations F12-0.1, F12-0.5 and F12-0.9 corresponding to different feedback parameters. We also show the evolution of the mean metallicity for the same runs (right-hand panels).

'Kennicutt law', since we have freedom only to adjust the overall efficiency of star formation; the slope and the surprisingly small scatter of the relation must emerge 'naturally' from the self-regulation of star formation within the numerical model. Below we show that our model can indeed reproduce the observed behaviour both for the simplified collapse model used in earlier sections and for an equilibrium galaxy model with structure similar to that of the Milky Way.

Our star formation algorithm assumes a star formation rate per unit volume equal to

$$\dot{\rho}_{\star} = c\,\frac{\rho}{\tau_{\rm dyn}}, \tag{7}$$

where $\rho_{\star}$ is the density of the new born stars, ρ is the gas density, $\tau_{\rm dyn}$ is the dynamical time of the gas, defined simply as $\tau_{\rm dyn} = 1/(4\pi G\rho)^{1/2}$, and c is a star formation efficiency parameter (see Paper I for details). In the numerical experiments analysed above, we used $c = 0.1$. In this section, we investigate the value required to reproduce the Kennicutt law by comparing our previous collapse model F12-0.5, with a virial mass of $10^{12}\,h^{-1}\,{\rm M}_{\odot}$, to an otherwise identical model where we lowered the star formation efficiency to $c = 0.01$. In the upper panel of Fig. 13 we show the resulting projected surface star formation rates and surface gas densities at three times, 0.5, 1.0 and 1.5 Gyr, averaging over broad annuli out to a radius of $30\,h^{-1}$ kpc. The observed Kennicutt relation is indicated on this plot by a dashed straight line. Clearly, for $c = 0.1$ (the open symbols) star formation is much more efficient in the simulation than is observed; disc gas is consumed rapidly, and there is considerable scatter about the mean relation. Reducing c by an order of magnitude reduces the star formation rates at given surface density by a similar factor, resulting in a much broader distribution of gas surface densities and an excellent fit to the zero-point slope and scatter of the observed relation. In addition, it is clear that as our idealized system builds up its disc it evolves along the Kennicutt relation. It is interesting that although star formation activity is reduced substantially for $c = 0.01$, the SN feedback model is still able to produce a strong galactic wind. After 1.5 Gyr of evolution, we find that $\sim$10 per cent of all baryons are both unbound and enriched with heavy elements.

The collapse initial conditions used here and above are highly idealized. In order to assess whether the apparent agreement with observation extends to quiescent star formation in an equilibrium system, we analyze two further simulations from initial conditions representing a spiral galaxy similar in structure to the Milky Way. The initial system is based on that studied in Springel, Di Matteo & Hernquist (2005). It consists of a dark matter halo, a stellar bulge, a diffuse hot-gas halo, and a disc with 10 per cent of its mass in gas and the rest in stars. The dark matter distribution is modelled

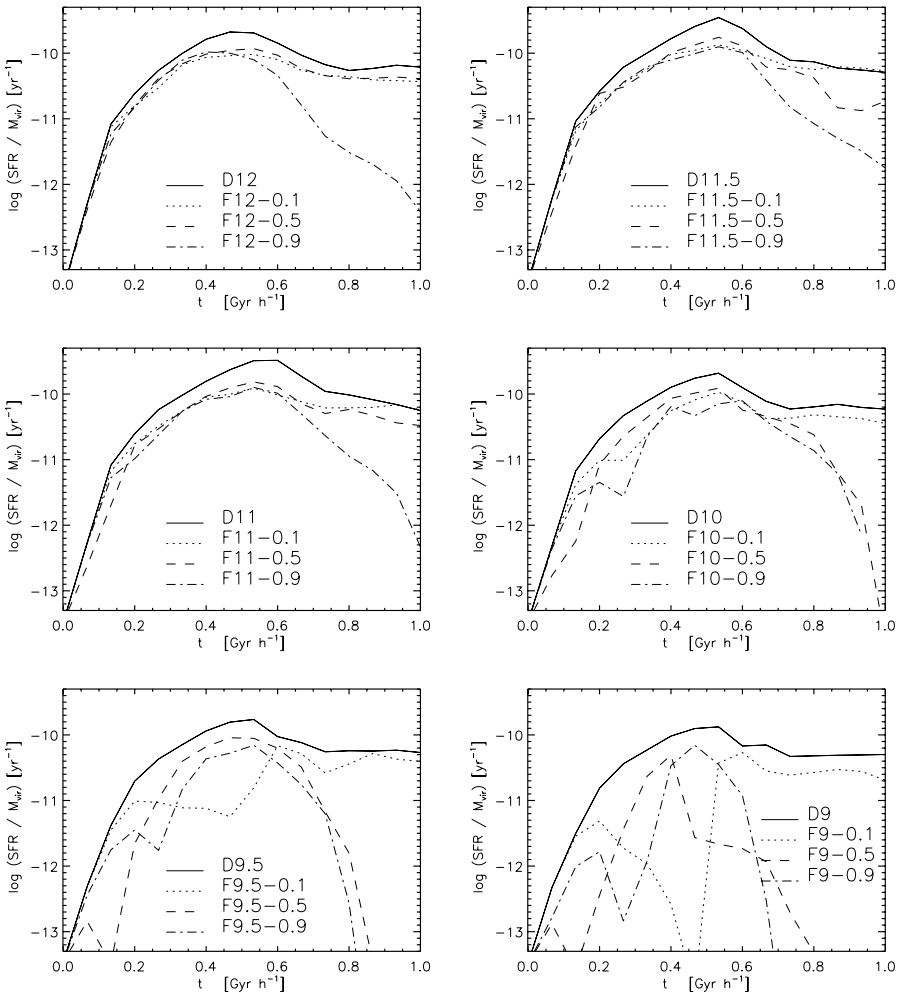

Figure 10. Star formation rates normalized to virial mass for simulations with total masses of 10^9, $10^{9.5}$, 10^{10}, 10^{11}, $10^{11.5}$ and $10^{12}\,h^{-1}\,\mathrm{M}_\odot$. The plots give results both for simulations without SN feedback (solid lines), and for simulations with SN feedback with $\epsilon_\mathrm{c} = 0.1$ (dotted lines), $\epsilon_\mathrm{c} = 0.5$ (dashed lines) and $\epsilon_\mathrm{c} = 0.9$ (dashed–dotted lines).

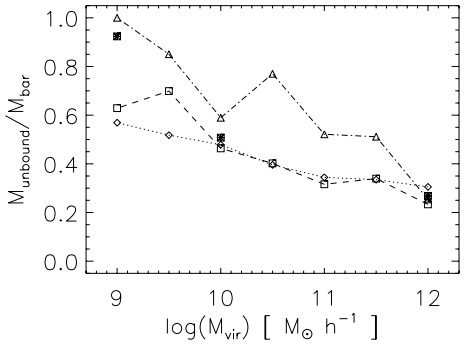

Figure 11. Fraction of unbound gas as a function of total baryonic mass for simulations with $\epsilon_\mathrm{c} = 0.1$ (dotted line), $\epsilon_\mathrm{c} = 0.5$ (dashed line) and $\epsilon_\mathrm{c} = 0.9$ (dashed–dotted line) after $0.85\,h^{-1}$ Gyr of evolution. We also show the results for our higher resolution simulations with $\epsilon_\mathrm{c} = 0.5$ (squared asterisks).

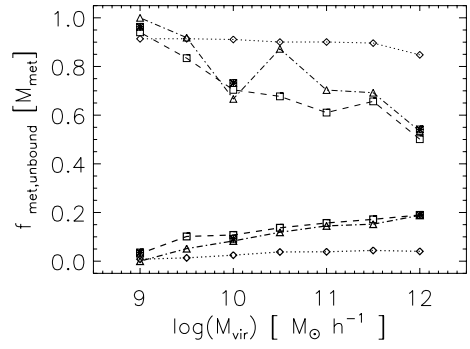

Figure 12. Fraction of metals locked into unbound gas (thin lines) and into stars (thick lines) as a function of total mass for simulations with $\epsilon_\mathrm{c} = 0.1$ (dotted lines), $\epsilon_\mathrm{c} = 0.5$ (dashed lines) and $\epsilon_\mathrm{c} = 0.9$ (dashed–dotted lines) after $0.85\,h^{-1}$ Gyr of evolution. We also show results for our higher resolution simulations with $\epsilon_\mathrm{c} = 0.5$ (squared asterisks).

as a spherical NFW distribution with a circular velocity at $r_{200} = 160\ h^{-1}\,\mathrm{kpc}$ of $161\,\mathrm{km\,s^{-1}}$ and a concentration parameter of 9 (Navarro, Frenk & White 1996, 1997). The disc has a radial scale-length of $2.5\,h^{-1}\,\mathrm{kpc}$, a vertical scale-height of $0.5\,h^{-1}\,\mathrm{kpc}$, and a Toomre stability parameter of $Q > 1$ for the stars. The spherical bulge is taken to have an exponential profile with scale-length 0.2 times that of the disc. The density of the hot gas follows that of the dark matter. The bulge, disc, hot-gas halo and dark matter halo are taken to have initial masses of 0.13, 0.39, 0.059 and $9.0 \times 10^{11}\,h^{-1}\,\mathrm{M}_\odot$, respectively. Initially dark matter, gas and stars are represented by

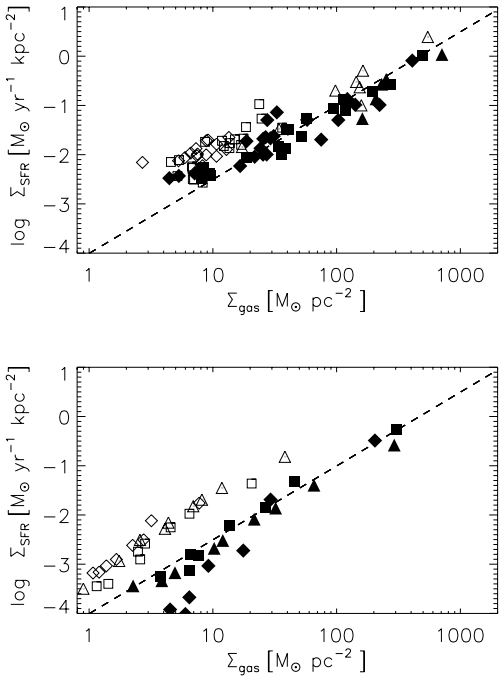

Figure 13. The upper panel shows projected star formation rate density as a function of gas surface density for two simulations of the collapse of a $10^{12}\,h^{-1}\,M_\odot$ mass system. Both surface densities are averaged over a series of annuli in face-on projections of the simulations. Open symbols refer to the model F12-0.5 discussed above at times 0.5 (triangles), 1.0 (squares) and 1.5 Gyr (diamonds), while corresponding filled symbols refer to the same times and to an otherwise identical model with $c = 0.01$. The lower panel shows results for two simulations from equilibrium initial conditions representing a spiral galaxy with structure similar to that of the Milky Way. The symbols refer to the same times and values of c as in the upper panel. The dashed line in both panels represents the relation of Kennicutt (1998).

simulation particles with mass 300, 2.0 and $15 \times 10^5\,h^{-1}\,M_\odot$, respectively. We have used gravitational softenings of 0.16, 0.32 and $0.2\,h^{-1}$ kpc for gas, dark matter and star particles, respectively. In these simulations, we assume that bulge and disc stars are old (i.e. they do not contribute to metal and energy ejection). Metals and SN energy are exclusively produced by the new stars which can be formed from the 10 per cent of the initial gas component. The system is set up in equilibrium and we followed its evolution using our full phase separation, star formation and feedback models with feedback parameters $\epsilon_r = 0$ and $\epsilon_c = 0.5$ and with $c = 0.1$ and $c = 0.01$. The star formation physics thus corresponds to the two versions of F12-0.5 compared above.

The lower panel of Fig. 13 shows the Kennicutt relations we find for these simulations at three different times. Despite the difference in initial conditions, the results resemble those found already for F12-0.5. For $c = 0.1$ the disc gas is used up quite rapidly (only 30, 17 and 11 per cent of the initial cold disc gas remains in the disc at the three times shown) and the star formation rates lie well above the empirical Kennicutt relation. With the lower star formation efficiency the observational relation is matched quite well and gas consumption times are lengthened (81, 67 and 54 per cent of the initial cold disc gas now remains in the disc at the three times shown). It is remarkable that even with the relatively modest star formation rates now found in this model, a significant galactic wind is generated. At the final time ($t = 1.5$ Gyr), 51 per cent of all metals formed are in the hot halo gas and 99 per cent of this gas is formally unbound and will likely leave the galaxy. Dividing this unbound mass by the age of the system leads to an estimated mass-loss rate in the wind of $6\,M_\odot\,yr^{-1}$ which can be compared with the mean star formation rate of $2\,M_\odot\,yr^{-1}$ averaged over the duration of the simulation. The ratio of these two rates is gratifyingly close to observational estimates for real wind-blowing galaxies (Martin 1999, 2004). The correct representation of the Kennicutt law found for $c = 0.01$ suggests this star formation efficiency as a good choice. The tests of this section confirm that our new SN-feedback model can match the observed phenomenology of star formation both during starburst episodes and during phases of quiescent star formation.

5 CONCLUSIONS

We have developed a new model for energy feedback by SNII and SNIa within the cosmological TreeSPH code GADGET-2, complementing the implementation of chemical enrichment and metal-dependent cooling described in Paper I. The model is tied to a multiphase treatment of the gas components in the ISM, designed to improve the description of the hot, diffuse material in the context of the SPH technique. One of the major advantages of our model is that no scale-dependent parameters need to be introduced. This makes it especially well suited for simulations of cosmological structure formation where systems of widely different mass form naturally.

We have used a number of idealized simulations of the formation of disc galaxies to study the performance of our numerical techniques. We found that our multiphase scheme leads to an improved description of the diffuse, hot gas which can reach densities up to an order of magnitude higher than those found with a standard SPH implementation of GADGET-2. The multiphase scheme is insensitive to its single free parameter α when the value is varied within a physically motivated range.

Our SNe feedback scheme efficiently regulates star formation by reheating cold gas and generating winds. The overall impact of SN feedback depends on total mass: in large systems the inclusion of feedback reduces star formation by a factor of a few compared to simulations where it is absent. Smaller systems are more strongly affected, with star formation reduced by more than an order of magnitude and occurring in stochastic starburst episodes. This finding is consistent with observational studies which detect bursty behaviour in the star formation activity of dwarf galaxies (e.g. Kauffmann et al. 2003; Tolstoy et al. 2003). In the simulations presented here, this behaviour has been achieved by applying our self-consistent multiphase gas and SN energy feedback schemes without introducing scale-dependent parameters. Furthermore, our SN feedback model can reproduce the Kennicutt relation between the surface densities of gas and of star formation both in collapsing and in quiescent systems.

For all the masses we considered, the star formation histories of our idealized protogalactic collapse models are sensitive to the fraction ϵ_c of energy and metals which is dumped into the cold phase. In general, the larger the value of ϵ_c, the more star formation is suppressed, but the effects of varying this parameter are complex because of the non-linear coupling between star formation, SN energy release, and radiative cooling.

Our SN feedback model results in strong winds from star-forming galaxies. The outflows are generally perpendicular to the disc plane and can reach velocities of up to 1000 km s^{-1}. We detect a clear anticorrelation between the unbound gas fraction and the total mass, indicating that the strength of the outflows is sensitive to the depth of the gravitational potential well, as expected from theoretical considerations. For a given total mass, we find that the unbound gas fraction

increases with the assumed value of the feedback parameter ϵ_c. The mass-loss rates we find typically exceed the star formation rates by a factor of a few, as observed in starbursting galaxies.

These winds are efficient in enriching the outer regions of our simulated galaxies and would plausibly contaminate the intergalactic medium. We found that the unbound gas component, regardless of total mass, ends up containing more than 60 per cent of the metals produced in our protogalactic collapses. For the smallest galaxies, this percentage goes up to 80 per cent or more, independent of the assumed value of ϵ_c. Galaxies with a wide range of masses may thus contribute to the enrichment of the intergalactic medium. This appears required to explain the observation that the bulk of the heavy elements in galaxy clusters resides in the intracluster medium rather than in the galaxies themselves. It will be extremely interesting to compute detailed predictions for this enrichment using cosmological simulations based on our feedback scheme.

ACKNOWLEDGMENTS

We thank the anonymous referee for a careful and constructive report. This work was partially supported by the European Union's ALFA-II programme, through LENAC, the Latin American European Network for Astrophysics and Cosmology. Simulations were run on Ingeld and HOPE PC-clusters at the Institute for Astronomy and Space Physics. We acknowledge support from Consejo Nacional de Investigaciones Científicas y Técnicas and Fundación Antorchas. CS thanks the Alexander von Humboldt Foundation, the Federal Ministry of Education and Research and the Programme for Investment in the Future (ZIP) of the German Government for partial support. The authors thank the Aspen Centre for Physics where part of the discussions of this work took place.

REFERENCES

Carraro G., Chiosi C., Girardi L., Lia C., 2001, MNRAS, 327, 69
Cen R., Ostriker J. P., 1992, ApJ, 399, L113
Cen R., Ostriker J. P., 1999, ApJ, 519, L109
Chiosi C., Carraro G., 2002, MNRAS, 335, 335
Croton D. J. et al., 2006, MNRAS, 365, 11
Dahlem M., Weaver K. A., Heckman T. M., 1998, ApJS, 118, 401
De Lucia G., Kauffmann G., White S. D. M., 2004, MNRAS, 349, 1101
Dekel A., Silk J., 1986, ApJ, 303, 39
Di Matteo T., Springel V., Hernquist L., 2005, Nat, 433, 604
Efstathiou G., 2000, MNRAS, 317, 697
Frye B., Broadhurst T., Benítez N., 2002, ApJ, 568, 558
Gallazzi A., Charlot S., Brinchmann J., White S. D. M., Tremonti C. A., 2005, MNRAS, 362, 41
Gerritsen J. P. E., Icke V., 1997, A&A, 325, 972
Gingold R. A., Monaghan J. J., 1977, MNRAS, 181, 375
Harfst S., Theis Ch., Hensler G., 2006, A&A, 449, 509
Hultman J., Pharasyn A., 1999, A&A, 347, 769
Katz N., 1992, ApJ, 391, 502
Katz N., Gunn J. E., 1991, ApJ, 377, 365
Kauffmann G. et al., 2003, MNRAS, 341, 54
Kay S. T., Pearce F. R., Frenk C. S., Jenkins A., 2002, MNRAS, 330, 113
Kennicutt R. C., 1998, ApJ, 498, 541
Larson R. B., 1974, MNRAS, 169, 229
Larson R. B., 1976, MNRAS, 176, 31
Lehnert M. D., Heckman T. M., 1995, ApJS, 97, L89
Lehnert M. D., Heckman T. M., 1996, ApJ, 462, 651
Lia C., Portinari L., Carraro G., 2002, MNRAS, 330, 821
Lucy L. B., 1977, ApJ, 82, 1013
Marri S., White S. D. M., 2003, MNRAS, 345, 561
Martin C. L., 1999, ApJ, 513, 156
Martin C. L., 2004, AAS, 205, 8901
Mayer L., Governato F., Colpi M., Moore B., Quinn T., Wadsley J., Stadel J., Lake G., 2001, ApJ, 547, L123
McKee C. F., Ostriker J. P., 1977, ApJ, 218, 148
Metzler C., Evrard A., 1994, ApJ, 437, 564
Mori M., Yoshii Y., Tsujimoto T., Nomoto K., 1997, ApJ, 478, L21
Nagashima M., Lacey C. G., Baugh C. M., Frenk C. S., Cole S., 2005, MNRAS, 358, 1247
Navarro J. F., White S. D. M., 1993, MNRAS, 265, 271
Navarro J. F., Frenk C. S., White S. D. M., 1996, ApJ, 462, 563
Navarro J. F., Frenk C. S., White S. D. M., 1997, ApJ, 490, 493
Pearce F. R. et al., 1999, ApJ, 521, 99
Pearce F. R., Jenkins A., Frenk C. S., White S. D. M., Thomas P. A., Couchman H. M. P., Peacock J. A., Efstathiou G., 2001, MNRAS, 326, 649
Rupke D. S., Veilleux S., Sanders D. B., 2002, ApJ, 570, 588
Scannapieco C., Tissera P. B., White S. D. M., Springel V., 2005, MNRAS, 364, 552 (Paper I)
Semelin B., Combes F., 2002, A&A, 388, 826
Shapley A. E., Erb D. K., Pettini M., Steidel C. C., Adelberger K. L., 2004, ApJ, 612, 122
Sommer-Larsen J., Gelato S., Vedel H., 1999, ApJ, 519, 501
Springel V., 2005, MNRAS, 364, 1105
Springel V., Hernquist L., 2002, MNRAS, 333, 649
Springel V., Hernquist L., 2003, MNRAS, 339, 289
Springel V., Di Matteo T., Hernquist L., 2005, MNRAS, 361, 776
Steinmetz M., Navarro J. F., 1999, ApJ, 513, 555
Sutherland R. S., Dopita M. A., 1993, ApJS, 88, 253
Thacker R. J., Couchman H. M. P., 2000, ApJ, 545, 728
Thacker R. J., Couchman H. M. P., 2001, ApJ, 555, L17
Thacker R. J., Tittley E. R., Pearce F. R., Couchman H. M. P., Thomas P. A., 2000, MNRAS, 319, 619
Thielemann F. K., Nomoto K., Hashimoto M., 1993, in Prantzos N., Vangoni-Flam E., Cassé N., eds, Origin and Evolution of the Elements. Cambridge Univ. Press, Cambridge, p. 299
Tissera P. B., De Rossi M. E., Scannapieco C., 2005, MNRAS, 364, L38
Tolstoy E., Venn K. A., Shetrone M., Primas F., Hill V., Kaufer A., Szeifert T., 2003, ApJ, 125, 707
Tremonti C. A., Heckman T. M., Kauffmann G., Brinchmann J., Charlot S. et al., 2004, ApJ, 613, 898
Trentham N., Tully R. B., 2002, MNRAS, 335, 712
White S. D. M., Frenk C. S., 1991, ApJ, 379, 52
White S. D. M., Rees M. J., 1978, MNRAS, 183, 341
Yepes G., Kates R., Khokhlov A., Klypin A., 1997, MNRAS, 284, 235

This paper has been typeset from a TEX/LATEX file prepared by the author.